Acta Pharmaceutica Sinica B 2025;15(8):4014−4029

Chinese Pharmaceutical Association
Institute of Materia Medica, Chinese Academy of Medical Sciences

Acta Pharmaceutica Sinica B

www.elsevier.com/locate/apsb
www.sciencedirect.com

ORIGINAL ARTICLE

The protein arginine methyltransferase PRMT1 ameliorates cerebral ischemia−reperfusion injury by suppressing RIPK1-mediated necroptosis and apoptosis

Tengfei Liu[a,†], Gan Huang[a,†], Xin Guo[a], Qiuran Ji[a], Lu Yu[a], Runzhe Zong[a], Yiquan Li[a], Xiaomeng Song[a], Qingyi Fu[a], Qidi Xue[a], Yi Zheng[d], Fanshuo Zeng[c], Ru Sun[b], Lin Chen[a,*], Chengjiang Gao[d,*], Huiqing Liu[a,c,*]

[a]*Department of Pharmacology, School of Basic Medical Sciences, Shandong University, Jinan 250012, China*
[b]*Department of Pharmacy, Shandong Provincial Hospital Affiliated to Shandong First Medical University, Jinan 250021, China*
[c]*Department of Rehabilitation Medicine, The Second Hospital, Cheeloo College of Medicine, Shandong University, Jinan 250033, China*
[d]*Key Laboratory of Infection and Immunity of Shandong Province & Department of Immunology, School of Basic Medical Sciences, Shandong University, Jinan 250012, China*

Received 23 January 2025; received in revised form 25 February 2025; accepted 14 April 2025

KEY WORDS

PRMT1;
Cerebral ischemia−reperfusion injury;
RIPK1;
Phosphorylation;
Arginine methylation;
Necroptosis;
Apoptosis;

Abstract Receptor-interacting protein kinase 1 (RIPK1) plays an essential role in regulating the necroptosis and apoptosis in cerebral ischemia-reperfusion (I/R) injury. However, the regulation of RIPK1 kinase activity after cerebral I/R injury remains largely unknown. In this study, we found the downregulation of protein arginine methyltransferase 1 (PRMT1) was induced by cerebral I/R injury, which negatively correlated with the activation of RIPK1. Mechanistically, we proved that PRMT1 directly interacted with RIPK1 and catalyzed its asymmetric dimethylarginine, which then blocked RIPK1 homodimerization and suppressed its kinase activity. Moreover, pharmacological inhibition or genetic ablation of PRMT1 aggravated I/R injury by promoting RIPK1-mediated necroptosis and apoptosis,

*Corresponding authors.
E-mail addresses: liuhuiqing@sdu.edu.cn (Huiqing Liu), cgao@sdu.edu.cn (Chengjiang Gao), linchen@sdu.edu.cn (Lin Chen).
[†]These authors made equal contributions to this work.

Peer review under the responsibility of Chinese Pharmaceutical Association and Institute of Materia Medica, Chinese Academy of Medical Sciences.

https://doi.org/10.1016/j.apsb.2025.06.005
2211-3835 © 2025 The Authors. Published by Elsevier B.V. on behalf of Chinese Pharmaceutical Association and Institute of Materia Medica, Chinese Academy of Medical Sciences. This is an open access article under the CC BY-NC-ND license (http://creativecommons.org/licenses/by-nc-nd/4.0/).

MLKL

while PRMT1 overexpression protected against I/R injury by suppressing RIPK1 activation. Our findings revealed the molecular regulation of RIPK1 activation and demonstrated PRMT1 would be a potential therapeutic target for the treatment of ischemic stroke.

© 2025 The Authors. Published by Elsevier B.V. on behalf of Chinese Pharmaceutical Association and Institute of Materia Medica, Chinese Academy of Medical Sciences. This is an open access article under the CC BY-NC-ND license (http://creativecommons.org/licenses/by-nc-nd/4.0/).

1. Introduction

Stroke is the second leading reason of death and physical disability among adults worldwide[1,2]. Ischemic stroke which is caused by the occlusion of carotid or cerebral arteries is the most common type of stroke[3]. Although the endovascular treatment, the only currently available therapeutic method, restores the blood supply and rescues the dying nerve cells, secondary ischemia−reperfusion (I/R) injury will further aggravate brain damage[4]. Hence, it is of great necessity to develop novel strategies to improve outcomes after cerebral I/R injury onset.

Receptor-interacting protein kinase 1 (RIPK1) plays an essential role in regulating cell death and neuroinflammation in cerebral I/R injury[5,6]. Necroptosis and apoptosis, 2 alternative programmed cell death, can be mediated by the activation of RIPK1. Under apoptosis-deficient or caspase-inhibited conditions, activated RIPK1 interacts with RIPK3 and promotes its activation, which in turn phosphorylates pseudokinase MLKL to execute necroptosis[7,8]. Under apoptosis-proficient conditions, the activation of RIPK1 promotes apoptosis by mediating the formation of complex IIa with FADD and caspase-8. Necroptosis seemed to be the earliest manner of programmed cell death during the cerebral I/R onset. In the middle cerebral artery occlusion (MCAO) model, it was noticed that the activation of RIPK1 sequentially promoted necroptosis followed by apoptosis in a temporally specific manner resulting from the degradation of TAK1[9]. Necrostatin-1 (Nec-1), the specific inhibitor of RIPK1 kinase activity, protects against neurological damage in ischemic stroke[10]. Meanwhile, a great deal of damage-associated molecular patterns were released due to RIPK1-mediated cell death, leading to inflammatory reactions and exacerbating I/R injury[5]. Therefore, regulating the kinase activity of RIPK1 has become an important strategy to alleviate cerebral I/R injury.

So far, the post-translational modifications of RIPK1 have been extensively studied which are vital in modulating RIPK1 signaling[11]. Autophosphorylation at ser166 is commonly used as a biomarker for RIPK1 activation[12]. Many E3 ligases and deubiquitinases including cIAP1/2, linear ubiquitin chain assembly complex, A20 and CYLD have been reported to regulate RIPK1 ubiquitination and then affect the downstream signaling[13-16]. However, it remains largely unknown how the kinase activity of RIPK1 is regulated after cerebral I/R injury.

Arginine methylation modification catalyzed by protein arginine methyltransferases (PRMTs) is another common post-translational modification. Methylarginine has 3 main types, mono-methylarginine (MMA), asymmetric dimethylarginine (ADMA) and symmetric dimethylarginine (SDMA)[17-19]. Notably, PRMT1 is the crucial member of type I methyltransferases that carry out the formation of MMA as an intermediate before the establishment of ADMA[20]. Accumulating studies have shown the relevance between PRMT1 and neurological disorders recently. PRMT1-specific depletion in the central nervous system impaired oligodendrocyte differentiation and remyelination[21,22]. SCY1-like pseudokinase 1 was methylated by PRMT1 which facilitated the formation of axon and dendrite structures[23]. PRMT1-mediated methylation of Fused in Sarcoma RNA-binding protein (FUS) was demonstrated to regulate its nucleus-cytoplasm shuttling, which was associated with aggregation of FUS in amyotrophic lateral sclerosis[24]. PRMT1 ablation in motor neurons caused age-related motor neuron degeneration with muscle loss[25]. However, whether PRMT1 is involved in cerebral I/R injury by regulating RIPK1 is unknown.

Here, we proved PRMT1 directly interacted with RIPK1 and catalyzed its ADMA, which then blocked RIPK1 homodimerization and kinase activation. Furthermore, we investigated the expression and biological function of PRMT1 in the cerebral I/R injury both *in vivo* and *in vitro*. We detected down-regulated PRMT1 and activated RIPK1 (p-S166 RIPK1) in neurons after acute ischemic insult. PRMT1 protects against I/R injury by blocking necroptosis and apoptosis by suppressing RIPK1 activation. Thus, PRMT1 would be a potential therapeutic target for the treatment of ischemic stroke.

2. Materials and methods

2.1. Animals

Male wild-type (WT) C57BL/6 mice (8−10 weeks, 23 ± 3 g, animal approval number: SCXK (Jing) 2019-0010) were purchased from SPF Biotechnology Ltd. (Beijing, China) *Prmt1*$^{flox/flox}$ mice were obtained from Professor Chengjiang Gao. *Thy1*-Cre mice with the mouse Thy-1 promoter-driven Cre recombinase was a gift from Dr. Bo Su. *Prmt1*$^{flox/flox}$ mice were crossed with *Thy1*-Cre mice to generate *Prmt1*$^{flox/flox}$ *Thy1*-Cre mice. Littermate *Prmt1*$^{flox/flox}$ mice were used as WT controls. The genotyping of *Prmt1*$^{flox/flox}$ was confirmed by PCR using the following primers: forward 5′-GTGCTTGCCATACAAGAGATCC-3′ and reverse 5′-ACAGCCGAGTAGCAAGGAGG-3′. The primers for *Thy1*-Cre transgenic mice genotyping were forward 5′-GCGGTCTGGCAG TAAAAACTATC-3′ and reverse 5′-GTGAAACAGCATTGCTG TCACTT-3′ and the primers for internal positive control were forward 5′-CTAGGCCACAGA ATTGAAAGATCT-3′ and reverse 5′-GTAGGT GGAAATTCTAGCATCATCC-3′. All *in vivo* experiments were approved by the Ethics Committee of Shandong University and performed in accordance to the principles outlined in the Institutional Animal Care and Use Committee of Shandong University (Jinan, China).

2.2. Brain adeno-associated virus delivery

Adeno-associated virus (AAV) 9 vectors encoding PRMT1 and corresponding empty vector (EV) were constructed by WZ Biosciences Inc. The neuron-specific promoter, human Synapsin I,

was utilized in the AAV-PRMT1 construct for high expression of PRMT1. WT mice were anesthetized and then placed on a stereotaxic apparatus. The left cortical injection of 2 μL of AAV-PRMT1 or AAV-EV suspension (1.0×10^{13} vg/mL) was carried out at a rate of 0.4 μL/min. The following coordinates were practiced: point 1, 0.3 mm anterior to the bregma, 2.3 mm lateral to the midline, 2 mm ventral to the dura; point 2, 1.8 mm posterior to the bregma, 2 mm lateral to the midline, 2 mm ventral to the dura.

2.3. Generation of cerebral I/R injury

Middle cerebral artery occlusion (MCAO) was executed upon WT mice to generate the cerebral I/R injury as described previously[26,27]. A substantial decrease to <20% of the baseline in the regional cerebral blood flow was determined as a successful occlusion. The mice subjected to 2 h of MCAO and indicated time reperfusion were euthanized. Animals in the sham group were subjected to the same procedure except for MCAO.

2.4. Neurological function and infarct volume assessment

To determine the outcome after MCAO, a 4-tiered neurological scoring system was employed in a blinded way as previously described[28]. The brains were sliced into 2 mm thick coronal sections. 2,3,5-Triphenyltetrazolium chloride (TTC) (Sigma, St. Louis, MO, USA) staining was used to determine the brain infarct size. Subsequently, the slices were incubated with 0.2% TTC (dissolved in PBS) for 30 min at a temperature of 37 °C and kept in 4% paraformaldehyde (Sigma). Every slice was photographed and infarct volumes were calculated across each section and presented as a percentage relative to the area of the contralateral hemisphere.

2.5. Corner tests

The corner test was performed as described previously[29]. In brief, the experimental corner setup was composed of 2 boards arranged to form a 30° corner, and a small opening was left along the joint between the 2 boards. The mouse was allowed to walk into the corner so that the vibrissae on both sides of the animal's face contacted the 2 boards simultaneously. Each mouse took part in 10 trials, after which we calculated the percentage of turns to each side.

2.6. Rotarod test

The motor coordination ability of mice was performed with rotarod apparatus (Panlab Harvard Apparatus, USA). In the training session, mice were placed towards the inside of the rotarod device at a constant 10 rpm for 200 s. In the test session, mice were placed on the rotarod device at an accelerating speed (starting from 0 to 45 rpm in 450 s). Speed and the duration until mice fell onto the base were recorded and only one trial was conducted[30].

2.7. Primary neuronal culture

The primary neuronal culture was performed as described previously[31]. E15 embryos in mice were collected and washed with D-Hanks buffer in dishes. Primary neuronal cells were plated on poly-D-lysine hydrobromide-coated glass coverslips in 12-well plates at a density of 600,000 cells/well in Neurobasal medium (Gibco Life Technologies, Grand Island, CA, USA) supplemented with B27 (Gibco Life Technologies) and GlutaMax (Gibco Life Technologies).

2.8. Histopathology

Mice brains were fixed in 4% paraformaldehyde and embedded in paraffin. Brain sections of 3 μm thickness were cut and stained with HE staining (Solarbio, Beijing, China) for visualization of the neuronal morphology in the cerebral cortex and hippocampus.

2.9. Cell culture, transfection, oxygen-glucose deprivation, and reoxygenation (OGD/R) procedure

HEK 293T cells and PC12 cells purchased from the Cell Center of Chinese Academy of Sciences (Shanghai, China) were cultured in DMEM (Meilunbio, Dalian, China) with 10% FBS. Lipofectamine 2000 (Invitrogen, Waltham, MA, USA) was utilized to transfect the indicated cells with plasmid or siRNA. The Reagents are listed in Supporting Information Table S1. The plasmids encoding GFP-PRMT1, Flag-PRMT1, Flag-PRMT1(VLD-AAA) and HA-ubiquitin were provided by Prof. Chengjiang Gao[32]. The Flag-His-RIPK1 expression plasmids were generated by WZ Biosciences Inc. (Jinan, China). The Myc-RIPK1 expression plasmids were obtained from Miaoling Biology (Wuhan, China). siRNAs were listed in Supporting Information Table S2. PC12 cells were incubated with EBSS solution for 3 h under 5% CO_2 and 95% N_2 at 37 °C for the deprivation of oxygen and glucose (OGD) and then switched back to indicated time reoxygenation.

2.10. Immunofluorescence staining

The slides of cells or frozen brain sections (10 μm) were double labeled with indicated primary antibodies at 4 °C overnight, and then incubated with the secondary antibodies for 2 h at room temperature. DAPI (Beyotime, Beijing, China) was used for nuclear labeling. Antibodies and dilution ratio used in immunofluorescence staining were listed in Supporting Information Table S3.

2.11. Cell viability measurement

The cell counting kit-8 (Beyotime) was used to determine the viability of PC12 cells.

2.12. TUNEL staining and PI staining

TUNEL staining was performed by an *in situ* cell death detection kit (KeyGen Biotech, Nanjing, China). Cell death analysis was also performed by propidium iodide (PI) (MedChem Express, Monmouth Junction, NJ, USA) staining. The number of TUNEL-positive or PI-positive cells was counted in 3 non-overlapping microscopic fields of view by a blinded researcher under high-power magnification (200×) and displayed as a percentage.

2.13. Measurement of apoptosis by flow cytometry

Flow cytometry was performed by the Annexin V-APC/PI apoptosis detection kit (Vazyme, Nanjing, China) according to the manufacturer's instructions. Cells in the Q1-UR and Q1-LR quadrant were determined as apoptotic cells.

2.14. Western blot and immunoprecipitation

Western blot analysis was performed as previously described[33]. For immunoprecipitation (IP), cells were collected and lysed with NP40 buffer for 30 min on the ice. Cell lysates were centrifuged and the supernatants were collected. The indicated antibodies and corresponding IgG controls were added into the supernatants and incubated for 4 h at 4 °C. Then protein A + G agarose (Santa Cruz, Dallas, TX, USA) was mixed rotarily overnight at 4 °C. Finally, the beads were washed and eluted in SDS−PAGE sample loading buffer. Antibodies and dilution ratio used in Western blot and IP assay were listed in Table S3.

2.15. Quantitative real-time PCR

RNA-quick purification kit (ES Science, Shanghai, China) was used to extract total RNA. 1 μg of total RNA was reverse-transcripted into cDNA using Hiscript II Q RT SuperMix (Vazyme). The PCR reaction was carried out using SYBR green qPCR mix (CWBio, Taizhou, China) on StepOne real-time PCR system. Primers were listed in Supporting Information Table S4.

2.16. Statistical analysis

Data were represented as mean ± standard deviation (SD) and analyzed using Prism software (Version 8.0) (GraphPad Software Inc, San Diego, CA, USA). Mean data between 2 experimental groups were compared using unpaired *t*-test. One-way or two-way ANOVA with *post hoc* Tukey's test was used to determine statistical differences among multiple groups. $P < 0.05$ was considered statistically significant.

3. Results

3.1. The protein level of PRMT1 was downregulated after cerebral I/R injury, which negatively correlated with p-RIPK1 (S166)

Previous studies indicated that arginine methylation extensively participated in neurological disorders. To investigate whether arginine methylation was involved in the cerebral I/R injury, we first monitored total ADMA, SDMA, and MMA levels. Surprisingly, the total ADMA level rather than SDMA or MMA significantly decreased in the brain tissues subjected to MCAO/R (Fig. 1A). Furthermore, the downregulation of ADMA alteration was also confirmed in PC12 cells stimulated by OGD/R (Fig. 1B). PRMT1 is the most predominant type I PRMTs in mammalian cells accounting for 85% of cellular PRMT activity[34]. Next, we evaluated the protein expression of PRMT1 in the brain of WT mice subjected to 2 h of MCAO followed by reperfusion for indicated time. The results showed that the protein level of PRMT1 was markedly decreased from 6 h till 48 h after reperfusion (Fig. 1C), and there was no alteration in the mRNA level of *Prmt1* at 6 h of reperfusion (Supporting Information Fig. S1). Meanwhile, the downregulation of PRMT1 was confirmed by immunofluorescence (Fig. 1D). Moreover, PRMT1 was mainly detected in NeuN-positive neurons (Fig. 1D) rather than Iba1-positive microglia (Supporting Information Fig. S2A) or GFAP-positive astrocytes (Fig. S2B). RIPK1 is a pivotal regulator of necroptosis and apoptosis in cerebral I/R injury, then we examined RIPK1 kinase activity and two major downstream cell death pathways mediated by activated RIPK1. p-RIPK1(S166), the biomarker of RIPK1 activation, was rapidly elevated at 3 h after reperfusion and reached a peak around 12 h in the ischemic brain tissue of WT mice (Fig. 1E). p-MLKL(S345) protein levels in I/R brain tissues were elevated from 3 h until 12 h after reperfusion (Fig. S2C). Cleaved-caspase 3 was obviously increased at 24 and 48 h after reperfusion (Fig. S2D). The results were in line with the previous study that the activation of RIPK1 sequentially promoted necroptosis followed by apoptosis after cerebral I/R[9]. Notably, the PRMT1 expression negatively correlated with p-RIPK1(S166) protein level in ischemic brain tissues (Fig. 1F). In addition, the protein level of PRMT1 was also greatly decreased in PC12 cells subjected to 3 h of OGD and 3, 6, 12, and 24 h of reoxygenation (Fig. 1G) while p-RIPK1(S166) (Fig. 1H), p-MLKL(S345) (Fig. S2E) and cleaved-caspase 3 (Fig. S2F) were elevated at varying time. Consistently, PRMT1 protein level was decreased in cultured primary neurons after OGD/R treatment (Supporting Information Fig. S3). Similarly, there was a negative correlation between PRMT1 and p-RIPK1(S166) protein levels in PC12 cells stimulated by OGD/R (Fig. 1I). These results suggested that PRMT1 may participate in cerebral I/R injury and be linked to the kinase activity of RIPK1. Hence, we further explored the role of PRMT1 on the kinase activity of RIPK1. It was demonstrated that the kinase activity of RIPK1 was greatly enhanced by PRMT1 knockdown (Fig. 1J). Consistently, PRMT1 overexpression dampened the phosphorylation level of RIPK1 at Ser166 dose-dependently (Fig. 1K).

3.2. Pharmacological inhibition of type I methyltransferase and genetic knockdown of PRMT1 enhanced necroptosis and apoptosis of PC12 cells induced by OGD/R

Based on our results that PRMT1 was altered in ischemic brain tissues and efficiently inhibited the kinase activity of RIPK1, we then investigated the role of PRMT1 in cerebral I/R injury. MS023 was used to inhibit the catalytic activity of PRMT1 and reduce ADMA modification[35]. The results showed that MS023 significantly suppressed cell viability of PC12 cells after 3 h of OGD and reoxygenation for 24 h (Supporting Information Fig. S4). Moreover, MS023 further increased the percentage of TUNEL-positive cells (Fig. 2A) and the ratio of apoptotic cells (Fig. 2B). Consistently, PRMT1 knockdown further exacerbated cell death induced by OGD/R evidenced with the reduction of cell viability (Supporting Information Fig. S5) and the increment of apoptosis (Fig. 3A). To uncover the PRMT1 effects on the kinase activity of RIPK1, we chose 6 h after reoxygenation as the optimal timing to examine p-RIPK1(S166) and p-MLKL(S345) and 24 h after reoxygenation for cleaved-caspase 3 examination according to our aforementioned data (Fig. 1). Notably, both MS023 and PRMT1 knockdown further elevated the protein levels of p-RIPK1 (S166), p-MLKL(S345) and cleaved-caspase 3 compared with the control group after OGD/R in PC12 cells (Figs. 2C−E, 3B−D). Moreover, we performed gene silencing for PRMT1 by lentiviral vectors (shPRMT1 sequence GCCUACUUCAACAUCGAGU) in cultured primary neurons, and similar results were obtained (Supporting Information Fig. S6).

To verify whether PRMT1 protected PC12 cells against OGD/R injury by regulating the kinase activity of RIPK1, we used a selective inhibitor of RIPK1 kinase Nec-1. Results revealed that Nec-1 restrained the increment of p-RIPK1 (S166), p-MLKL (S345), and cleaved-caspase 3 induced by PRMT1 silence in OGD/R-treated PC12 cells (Fig. 3E−G). Moreover, Nec-1 rescued

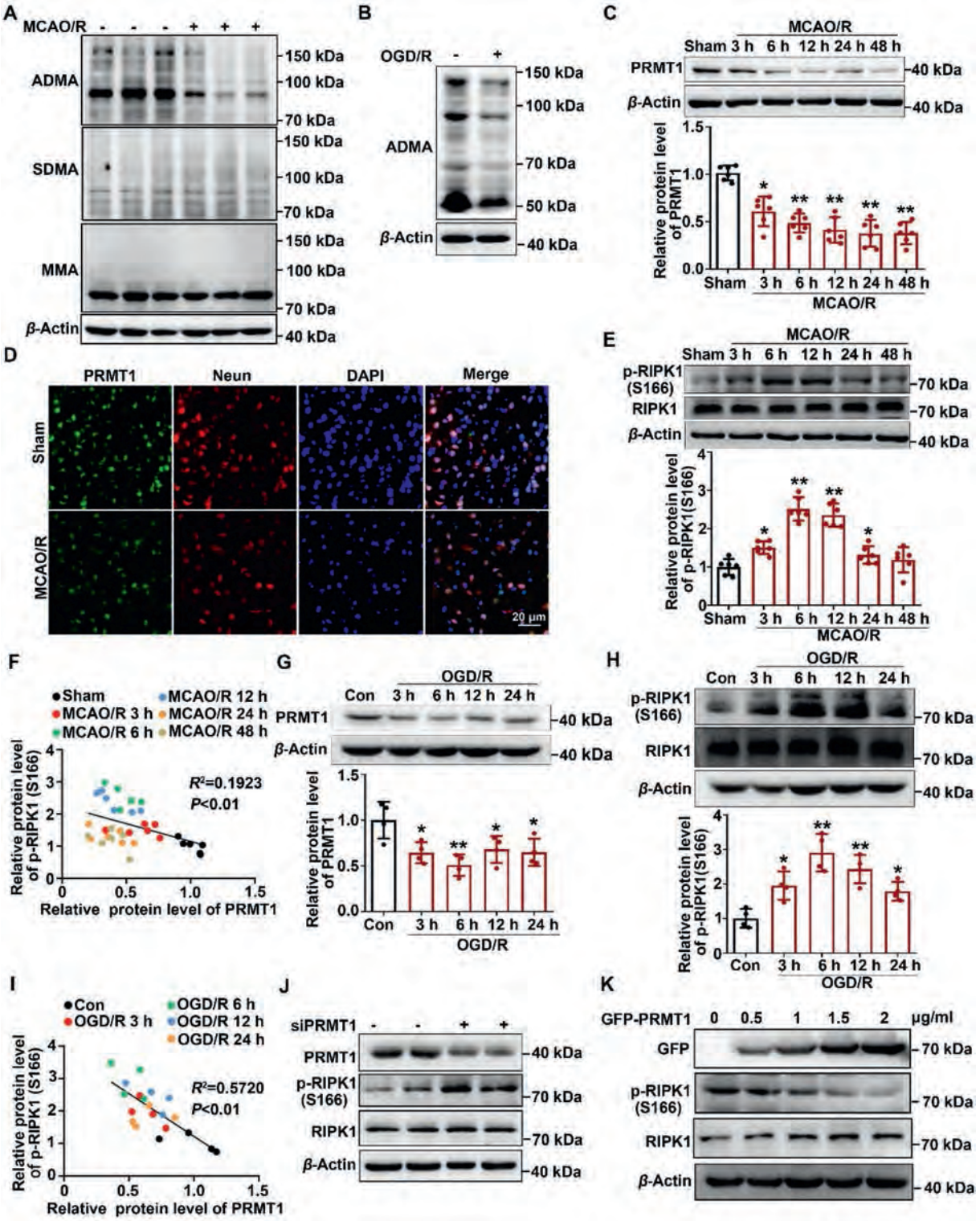

Figure 1 The protein level of PRMT1 was downregulated after cerebral I/R injury, which negatively correlated with p-RIPK1(S166). (A) Western blot analysis of the total ADMA, SDMA, and MMA in brain tissues from wild-type (WT) mice subjected to middle cerebral artery occlusion (MCAO) for 2 h and reperfusion for 24 h. (B) Western blot analysis of the total ADMA in PC12 cells subjected to OGD/R. Western blot analysis of PRMT1 (C), p-RIPK1 (S166), and RIPK1 (E) in brain tissues from WT mice after MCAO for 2 h and reperfusion for 3, 6, 12, 24, and 48 h, $n = 6$ mice per group. (D) Double immunofluorescence of PRMT1 (green) and NeuN (neuron marker, red) was performed in mouse ischemic cortex after 2 h MCAO and 12 h reperfusion. Scale bar, 20 μm. Western blot analysis of PRMT1 (G), RIPK1, and p-RIPK1 (S166) (H) in PC12 cells subjected to OGD for 3 h and reoxygenation for 1, 3, 6, 12, and 24 h. (F, I) Pearson correlation analyses showing the correlations between PRMT1 and p-RIPK1 (S166) expression in the brain of WT mice subjected to MCAO/R (F) or PC12 cells subjected to OGD/R (I), $P < 0.01$ for all of these correlations. (J) Western blot analysis of PRMT1, p-RIPK1 (S166), and RIPK1 in PC12 cells transfected with siPRMT1

the cell death induced by PRMT1 silence markedly in OGD/R-treated PC12 cells as shown by the cell viability test and PI staining (Fig. 3H and I). Hence, these data suggested that inhibition of PRMT1 aggravated necroptosis and apoptosis in PC12 cells induced by OGD/R by promoting RIPK1 activation.

3.3. PRMT1 overexpression inhibited RIPK1-mediated necroptosis and apoptosis in PC12 cells subjected to OGD/R

The plasmid encoding PRMT1 was transfected into PC12 cells subjected to OGD/R to further confirm the function of PRMT1 in cerebral I/R. It was demonstrated that PRMT1 overexpression increased the cell viability of PC12 cells after OGD/R (Supporting Information Fig. S7). In addition, TUNEL staining results revealed that PRMT1 overexpression markedly reduced the ratio of TUNEL-positive cells induced by OGD/R (Fig. 4A). Cell apoptosis induced by OGD/R was greatly suppressed by PRMT1 overexpression as shown by flow cytometry analysis (Fig. 4B). Meanwhile, PRMT1 overexpression efficiently inhibited the protein levels of p-RIPK1 (S166), p-MLKL (S345) and cleaved-caspase 3 after OGD/R stimulation (Fig. 4C−E). Taken together, these data suggested that PRMT1 alleviated OGD/R-induced necroptosis and apoptosis in PC12 cells by inhibiting RIPK1 activation.

3.4. PRMT1 interacted with RIPK1 directly

PRMT1 alleviated OGD/R injury by inhibiting RIPK1 activation, then we investigated the underlying mechanism by which PRMT1 regulated RIPK1 activity. The co-immunoprecipitation (Co-IP) results clearly showed that PRMT1 interacted with RIPK1 (Fig. 5A and B). Meanwhile, immunofluorescence results suggested obvious co-localization between PRMT1 and RIPK1 (Fig. 5C). Consistently, the interaction between endogenous PRMT1 and RIPK1 was observed in PC12 cells and reduced after OGD/R (Fig. 5D). Furthermore, we purified recombinant proteins, and the pull-down experiment *in vitro* confirmed the direct interaction between PRMT1 and RIPK1 (Fig. 5E). Overall, these data indicated that PRMT1 directly targeted RIPK1.

3.5. PRMT1 inhibited RIPK1 autophosphorylation by promoting its methylation at R658

Given that PRMT1 is the most predominant methyltransferase in mammalian cells, we determined whether PRMT1 regulated the arginine methylation of RIPK1. The plasmids encoding WT PRMT1 or the activity mutant PRMT1 (VLD-AAA)[36] were transfected into PC12 cells and the protein level of p-RIPK1 (S166) was detected. Notably, the overexpression of WT PRMT1 rather than PRMT1 (VLD-AAA) led to a significant reduction in RIPK1 phosphorylation (Fig. 6A). These data indicated that the methyltransferase activity of PRMT1 was required for regulating the kinase activity of RIPK1. Then we assessed whether PRMT1 could promote the asymmetric arginine methylation of RIPK1 and found that the methylation of RIPK1 was readily detected, especially the ADMA modification (Fig. 6B). Besides, ADMA modification of RIPK1 was reduced in PC12 cells subjected to OGD/R (Fig. 6C). Notably, the formation of ADMA in RIPK1 was significantly dampened in PC12 cells treated by MS023 (Fig. 6D) and PRMT1 knockdown (Fig. 6E). Consistently, we observed that RIPK1 arginine methylation was upregulated in the presence of Flag-PRMT1 (WT), but not in the presence of its mutant Flag-PRMT1 (VLD-AAA) (Fig. 6F). The homodimerization of RIPK1 is vital for the autophosphorylation of RIPK1 and its downstream signaling necroptosis and apoptosis[37]. To further confirm the role of arginine methylation in the formation of RIPK1 dimers, we transfected Flag-RIPK1 and Myc-RIPK1 plasmids into HEK 293T cells in the presence or absence of GFP-PRMT1. Co-IP analysis showed that PRMT1 attenuated the dimerization of RIPK1 (Fig. 6G). Consistently, confocal microscopy analysis revealed that RIPK1 exhibited obvious aggregated punctate staining, while PRMT1 overexpression markedly reduced the dots (Fig. 6H), suggesting that PRMT1 likely regulated the RIPK1 aggregation. Previous studies demonstrated the ubiquitination of RIPK1 plays an essential part in the formation of complex I and regulating RIPK1 kinase activity as well[11]. However, our results indicated that PRMT1 overexpression did not harbor any change in the ubiquitination of RIPK1 (Fig. 6I).

To identify the arginine residue(s) that is methylated by PRMT1, we analyzed the protein sequence of RIPK1 using methylation prediction tools GPS-MSP[38]. Three arginine residues ranked top scores were selected for further analyses (Supporting Information Fig. S8A and S8B). We substituted R71, R371, and R658 residues in Myc-RIPK1 with lysine (K) individually and the methylation status of RIPK1 was examined. The result showed that the substitution of R658 to K (R658K) completely blocked ADMA modification of RIPK1 induced by PRMT1(Fig. 6J). Next, we detected whether PRMT1 regulated the kinase activity of RIPK1 by catalyzing its arginine methylation at R658. Myc-RIPK1^{WT} and Myc-RIPK1^{R658K} plasmids were transfected into HEK 293T cells together with GFP-PRMT1. The IP results showed that PRMT1 overexpression decreased the p-RIPK1 (Ser166) level of RIPK1^{WT} rather than Myc-RIPK1^{R658K} (Fig. 6K). Moreover, we further investigated whether PRMT1 protected neurons against I/R injury by regulating ADMA modification of RIPK1 at R658 residue. Previous studies reported that RIPK1 deficiency did not affect cell survival obviously under normal conditions[39,40]. Thus, we silenced the endogenous RIPK1 expression using siRNA (Fig. S8C) and then transfected the resistant Myc-RIPK1^{WT} or Myc-RIPK1^{R658K} plasmids into PC12 cells subjected to OGD/R in the presence or absence of GFP-PRMT1. The results showed that PRMT1 overexpression obviously increased cell viability, reduced the rate of PI^{+} cells, and inhibited p-RIPK1 (S166) protein level and its downstream signals in PC12 cells transfected with Myc-RIPK1^{WT} after OGD/R, while it did not affect the cells transfected with Myc-RIPK1^{R658K} (Fig. S8D−S8H). These data indicated that PRMT1 displayed its neuroprotective effects by catalyzing RIPK1 arginine methylation at R658.

3.6. Pharmacological inhibition or genetic ablation of PRMT1 aggravated brain injury in mice subjected to MCAO/R

To further investigate the potential role of PRMT1 in cerebral I/R injury *in vivo*, MS023 was intraventricularly administered to mice 30 min before MCAO and reperfusion. Pretreatment with MS023

or negative control. (K) Western blot analysis of GFP-PRMT1, p-RIPK1 (S166), and RIPK1 in HEK 293T cells transfected with GFP-PRMT1 plasmid or empty vector. Results are representative of 4 independent experiments. Data are presented as mean ± SD. Multiple comparisons were evaluated by one-way ANOVA (C, E, G, H) followed by Tukey's test. $^{*}P < 0.05$, $^{**}P < 0.01$ compared with control group.

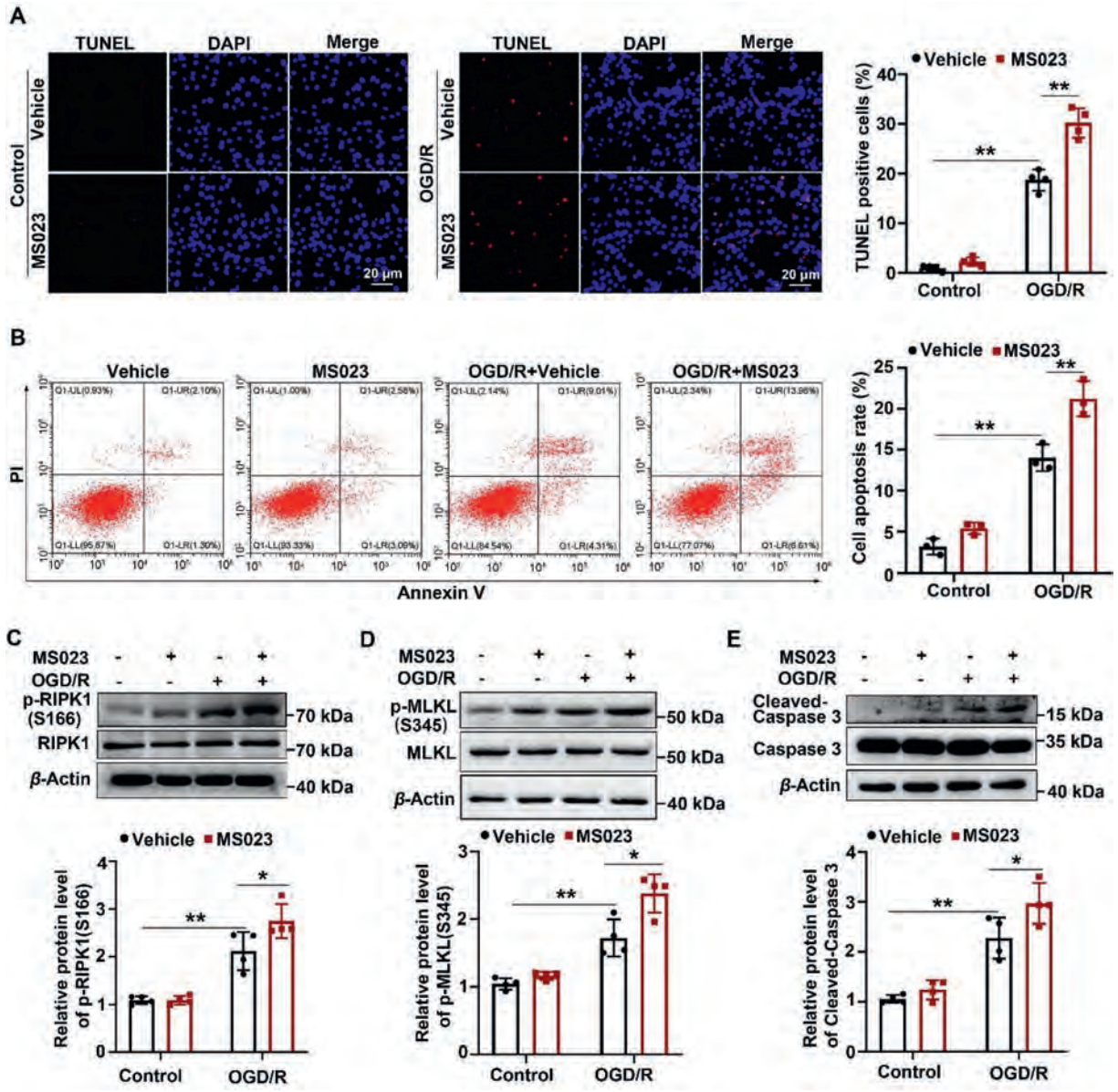

Figure 2 MS023, an inhibitor of type I protein arginine methyltransferase (PRMT), enhanced necroptosis and apoptosis of PC12 cells after OGD/R. PC12 cells were subjected to OGD for 3 h and reoxygenation for 24 h, 5 μmol/L MS023 or vehicle was administered during reoxygenation. TUNEL assay (A), flow cytometry analysis (B) and the protein levels of cleaved-caspase 3 and caspase 3 (E) were assessed. Western blot analysis of p-RIPK1 (S166) and RIPK1 (C), p-MLKL (S345) and MLKL (D) was determined in PC12 cells subjected to 3 h OGD and 6 h reoxygenation with MS023 treatment. Scale bars, 20 μm. Results are representative of 3 or 4 independent experiments. All data are shown as mean ± SD. Multiple comparisons were evaluated by two-way ANOVA followed by Tukey's test, $^{*}P < 0.05$, $^{**}P < 0.01$ compared with the indicated group.

obviously increased neurological deficit score (Fig. 7A) and infarction volume (Fig. 7B and C) induced by MCAO/R. Moreover, MS023 aggravated neuronal morphological lesions in the hippocampus and cortex visualized by H&E staining (Fig. 7D) and increased the TUNEL-positive cells substantially at 24 h after reperfusion (Fig. 7E). Subsequently, we found that MS023 further increased the protein levels of p-RIPK1 (S166), p-MLKL (S345) and cleaved-caspase 3 in I/R brain tissues (Fig. 7F, Supporting Information Fig. S9). Focal cerebral I/R triggers a robust inflammatory response involving the activation of microglia and astrocytes and the production of cytokines. Molecules released from cells undergoing necrosis also amplify the inflammatory response[41]. Our qPCR results revealed that MS023 significantly upregulated the mRNA levels of the proinflammatory cytokines including IL-1β, IL-6 and TNF-α in ischemic brain tissues after MCAO/R (Fig. 7G).

To strengthen the function of PRMT1 in cerebral I/R injury, we breed *Prmt1*$^{flox/flox}$*Thy1*-Cre mice to conditionally knockout (CKO) PRMT1 in neurons (Fig. 8A and B). Littermate *Prmt1*$^{flox/flox}$ mice were used as WT controls. We found *Prmt1*

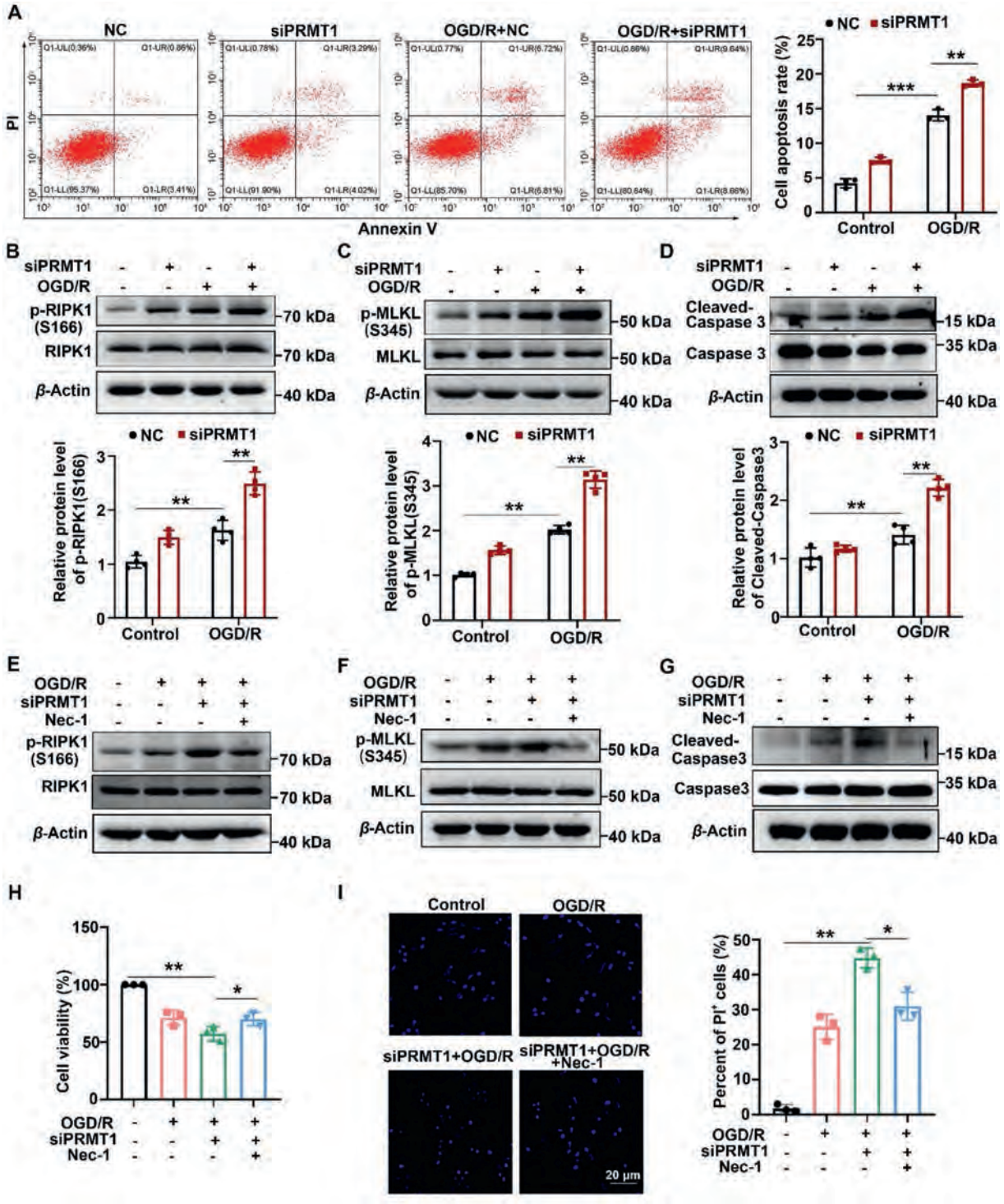

Figure 3 PRMT1 silence exacerbated RIPK1-mediated necroptosis and apoptosis of PC12 cells induced by OGD/R. PC12 cells transfected with siPRMT1 or NC were subjected to OGD for 3 h and reoxygenation for 24 h. In rescue experiments, PC12 cells were treated with 10 μmol/L Nec-1 during siPRMT1 transfection and OGD/R process. Flow cytometry analysis (A), PI staining (I), cell viability (H), and the protein levels of cleaved-caspase 3 and caspase 3 (D, G) were assessed. p-RIPK1 (S166) and RIPK1 (B, E), p-MLKL (S345) and MLKL (C, F) in PC12 cells subjected to 3 h of OGD and 6 h of reoxygenation were determined by Western blot. Results are representative of 3 or 4 independent experiments. All data are shown as mean ± SD. Multiple comparisons were evaluated by two-way ANOVA followed by Tukey's test, $^{*}P < 0.05$, $^{**}P < 0.01$, $^{***}P < 0.001$ compared with the indicated group.

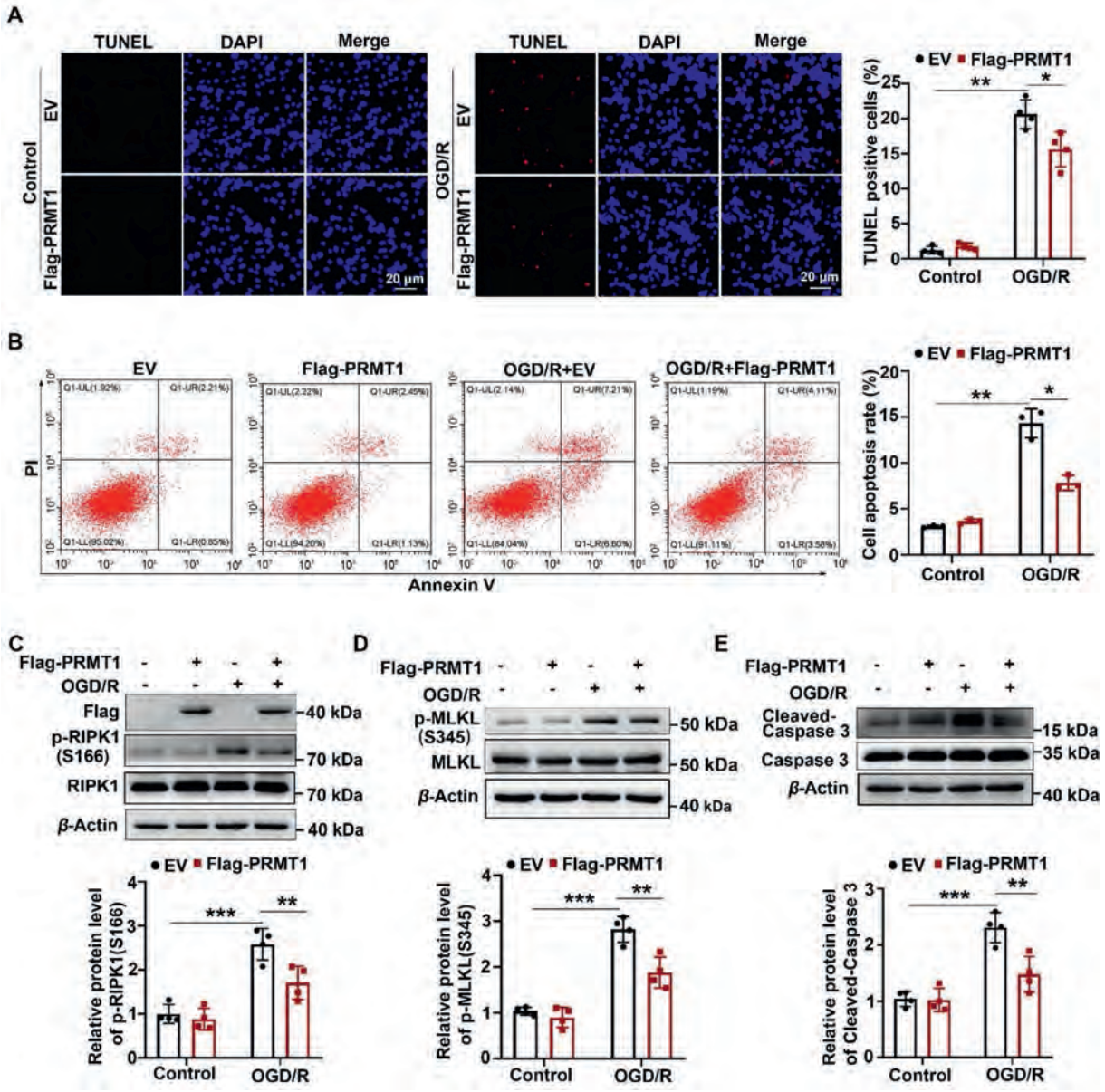

Figure 4 PRMT1 protected PC12 cells against OGD/R injury by inhibiting necroptosis and apoptosis. PC12 cells transfected with Flag-PRMT1 or empty vector (EV) were subjected to OGD for 3 h and reoxygenation for 24 h. TUNEL assay (A), flow cytometry analysis of Annexin V and PI (B), and the protein levels of cleaved-caspase 3 and caspase 3 (E) were assessed. p-RIPK1 (S166) and RIPK1 (C), p-MLKL (S345) and MLKL (D) in PC12 cells subjected to 3 h of OGD and 6 h of reoxygenation were determined by Western blot. Scale bars, 20 μm. Results are representative of 3 or 4 independent experiments. All data are shown as mean ± SD. Multiple comparisons were evaluated by two-way ANOVA followed by Tukey's test, $^{*}P < 0.05$, $^{**}P < 0.01$, $^{***}P < 0.001$ compared with the indicated group.

CKO mice were viable at birth and moved normally, but the body weight was approximately 13.1% less than that of littermate WT mice (Supporting Information Fig. S10). Then we performed 2 h MCAO and 24 h reperfusion on *Prmt1*^{CKO} mice and WT controls. It was observed that PRMT1 deficiency increased neurological deficit score (Fig. 8C), infarction volume (Fig. 8D and E), and the ratio of TUNEL-positive cells (Fig. 8F). Consistently, PRMT1 ablation further elevated the expression of p-RIPK1 (S166), p-MLKL (S345) and cleaved-caspase 3 (Fig. 8G–I). Collectively, these data indicated that pharmacological inhibition or genetic ablation of *Prmt1* exacerbated the cerebral I/R injury.

3.7. Overexpression of PRMT1 ameliorated the brain injury induced by MCAO/R

Based on the obvious downregulation of PRMT1 in neurons, we overexpressed PRMT1 by injecting AAV-PRMT1 into the brain of WT mice (Fig. 9A). The neuron-specific promoter, human synapsin I, was utilized in the AAV-PRMT1 construct for high expression of PRMT1. The efficiency of PRMT1 overexpression was evaluated by GFP fluorescence in brain sections (Fig. 9B) and Western blot analysis in cortical tissues (Fig. 9C). Results showed that PRMT1 overexpression significantly attenuated the cerebral

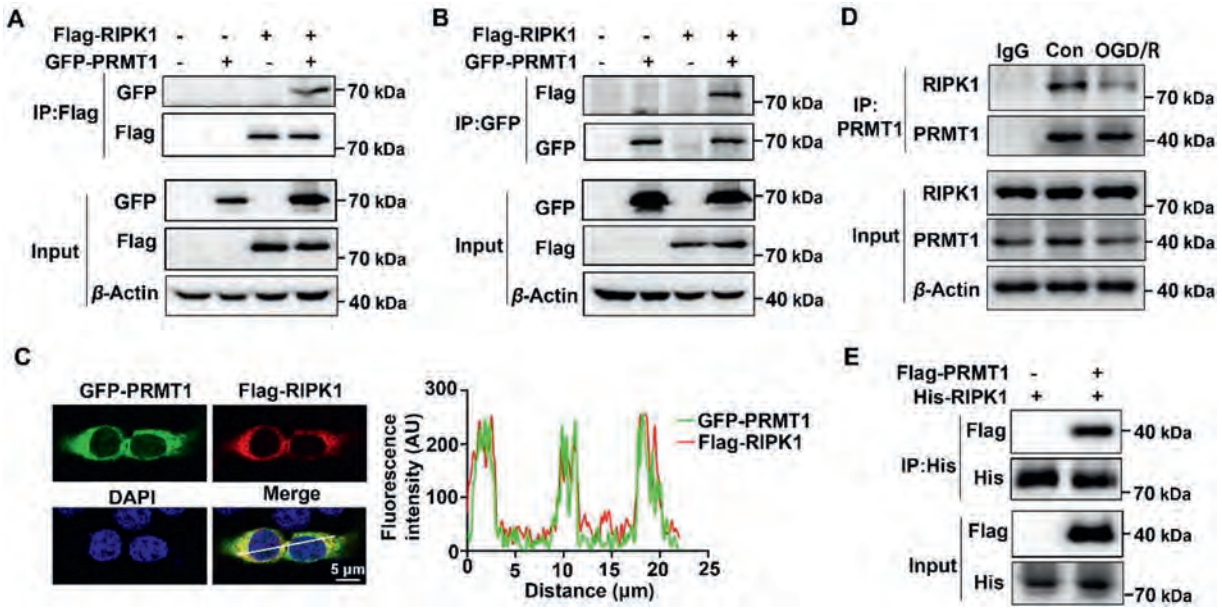

Figure 5 PRMT1 interacted with RIPK1 directly. (A, B) Co-IP analysis of the exogenous interaction of PRMT1 with RIPK1. HEK 293T cells were transfected with plasmids expressing GFP-PRMT1 and Flag-RIPK1. (C) Representative images of laser scanning confocal microscopy for GFP-PRMT1 (green) and Flag-RIPK1 (red) in HEK 293T cells. Scale bar, 5 μm. (D) Co-IP analysis of the endogenous interaction of PRMT1 with RIPK1 in PC12 cells subjected to 3 h of OGD and 6 h of reoxygenation. (E) Co-IP analysis of the interaction between recombinant protein Flag-PRMT1 and His-RIPK1 incubated *in vitro*.

I/R injury in mice subjected to MCAO/R (Fig. 9D−H, Supporting Information Fig. S11). Moreover, the ratio of TUNEL-positive cells was less in mice injected with AAV-PRMT1 than in mice injected with AAV vectors after MCAO/R (Fig. 9I). Meanwhile, PRMT1 overexpression restrained the activation of RIPK1 and its downstream signaling p-MLKL (S345) and cleaved-caspase 3 in I/R brain tissues (Fig. 9J, Supporting Information Fig. S12). Consistently, PRMT1 overexpression greatly downregulated the mRNA levels of the proinflammatory cytokines in ischemic brain tissues after MCAO/R (Fig. 9K).

4. Discussion

Accumulating studies highlighted the important role of RIPK1 as a central mediator of apoptosis and necroptosis following acute ischemic neuronal injury[9,10,42]. However, the regulation of RIPK1 kinase activity in ischemic stroke remains largely unknown. In this study, we proved that PRMT1 directly interacted with RIPK1 and catalyzed its ADMA modification, which then inhibited the dimerization and phosphorylation of RIPK1. The cerebral I/R injury triggered the downregulation of PRMT1, which promoted the activation of RIPK1 and exacerbated the brain damage. Furthermore, we provided evidence that PRMT1 protected against cerebral I/R injury by inhibiting RIPK1-mediated apoptosis and necroptosis.

RIPK1 is activated through autophosphorylation, especially at Ser166 residue[12]. RIPK1 phosphorylation by IKK1/2[43], MK2[44], and TAK1[45] was shown to prevent autophosphorylation and induce phosphorylation at other residues. Ubiquitination is another critical regulatory mechanism of RIPK1. K63-linked ubiquitination of RIPK1 by cIAP1/2 promoted complex I formation by facilitating the recruitment of TAK1, LUBAC, NEMO, IKK1/2, etc[13,14]. Deubiquitinase CYLD removed K63-linked and M1-linked ubiquitin chains from RIPK1 and promoted necroptosis onset[16,46]. E3 ligase PELI1 mediated K63-linked ubiquitination of RIPK1 at K115 residue which is required for the formation of necrosome[47]. Here, we provide the first proof that the phosphorylation of RIPK1 rather than its ubiquitination was suppressed by PRMT1-mediated arginine methylation. RIPK1 consists of an N-terminal kinase domain (KD), an intermediate domain (ID) containing a receptor-interacting protein homotypic interaction motif (RHIM) and a C-terminal death domain (DD)[7]. Previous structural studies showed that RIPK1-DD-mediated homodimerization promoted the autophosphorylation and activation of RIPK1[37]. We found that PRMT1 significantly reduced the dimerization of RIPK1 and inhibited the phosphorylation of RIPK1 at Ser166. It was reported that mutating K599R in human RIPK1 (K584 in murine RIPK1), a lysine located on the surface of the DD, blocked RIPK1 homodimerization and its kinase activation. The defect of K584R can be rescued by forced dimerization, which indicated that K599/K584 might be subject to modification, *e.g.*, methylation, and the modification was likely to affect RIPK1 dimerization[37]. Additionally, arginine methylation has been reported to contribute to the conformational changes[38]. Importantly, we demonstrated that PRMT1 regulated the kinase activity of RIPK1 by catalyzing its arginine methylation at R658 residue. Therefore, we proposed that arginine methylation of RIPK1^{R658} induced by PRMT1 would affect the DD-mediated RIPK1 homodimerization by changing its conformation. However, the exact spatial conformation changes caused by methylation need to be explored further.

PRMT1 is the leading member of type I PRMT which accounts for over 90% of ADMA[34]. The Human Protein Atlas (https://www.proteinatlas.org/) database showed that PRMT1 is extensively distributed in the nervous system. Previous studies revealed that PRMT1 played a dominant role in the development of the nervous system[22] and neurodegenerative diseases[25]. However,

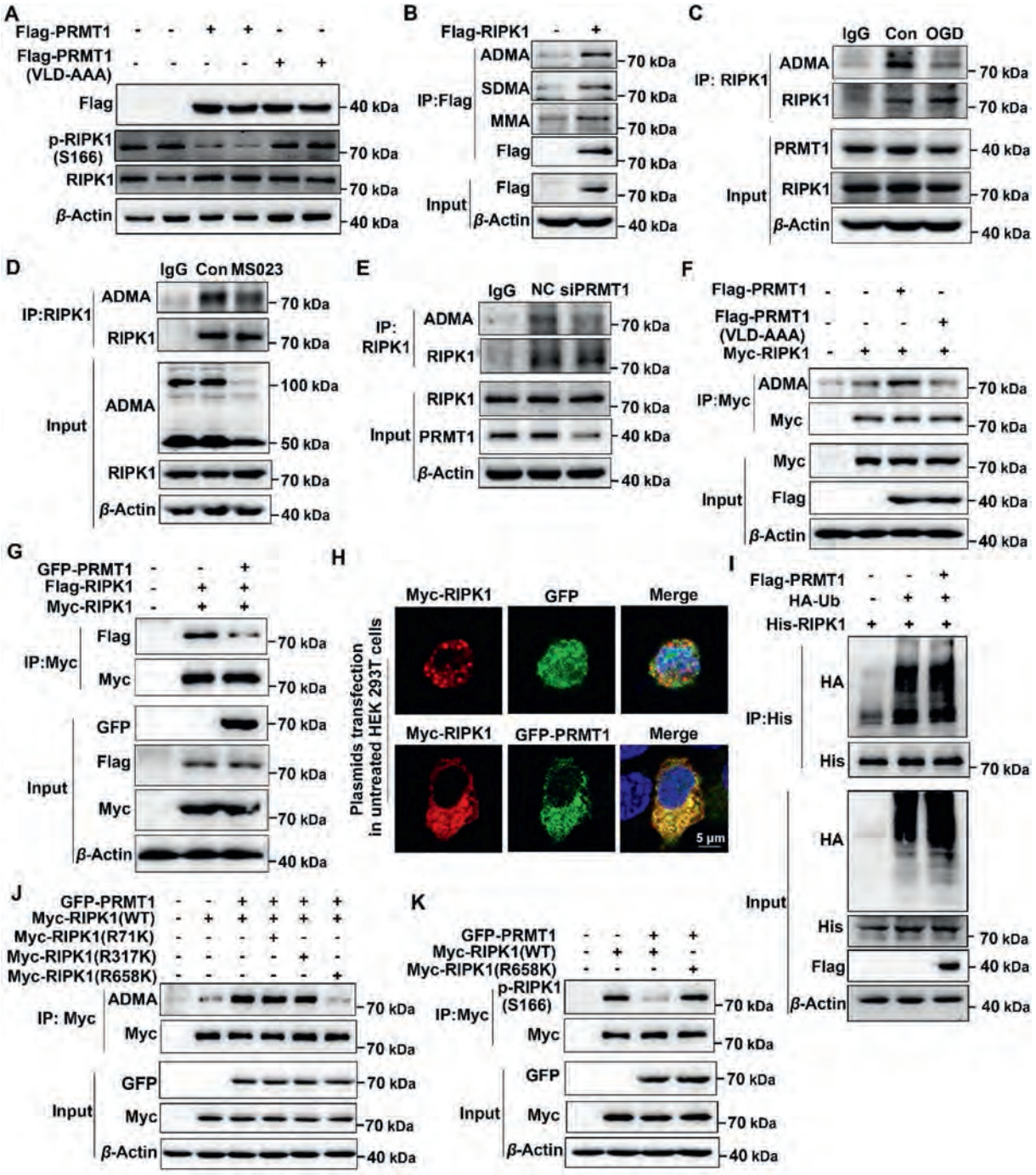

Figure 6 PRMT1 inhibited RIPK1 auto-phosphorylation by promoting its methylation. (A) Western blot analysis of Flag-PRMT1, p-RIPK1 (S166), and RIPK1 in PC12 cells transfected with Flag-PRMT1 plasmid (WT or VLD-AAA). (B) Co-IP analysis of arginine methylation types (ADMA, SDMA, MMA) of RIPK1 in HEK 293T cells transfected with plasmids expressing Flag-RIPK1. (C) Co-IP analysis of the endogenous RIPK1 asymmetric dimethylation in PC12 cells subjected to 3 h of OGD and 6 h of reoxygenation. (D) IP analysis of the ADMA level of RIPK1 in PC12 cells treated with vehicle or MS023 for 24 h. (E) IP analysis of the ADMA level of RIPK1 in PC12 cells transfected with siPRMT1 or NC. (F) IP analysis of the ADMA level of RIPK1 in HEK 293T cells transfected with Flag-PRMT1 plasmid (WT or VLD-AAA) and Myc-RIPK1. (G) HEK 293T cells were transfected with Flag-RIPK1, Myc-RIPK1 and GFP-PRMT1 plasmids. The interaction between differently tagged proteins was determined by Co-IP analysis. (H) Representative images of laser scanning confocal microscopy for GFP (green) and Myc (red) in HEK 293T cells transfected with Myc-RIPK1 and GFP-PRMT1 or GFP-vector plasmids. Scale bar, 5 μm. (I) IP analysis of RIPK1 ubiquitination in HEK 293T cells transfected with plasmids expressing Flag-PRMT1, His-RIPK1, and HA-ubiquitin (HA-Ub). (J) IP analysis of the ADMA level of RIPK1 in HEK 293T cells transfected with plasmids expressing GFP-PRMT1, Myc-RIPK1^{WT}, or corresponding mutants. (K) IP analysis of the phosphorylation level (Ser166) of RIPK1 in HEK 293T cells transfected with plasmids expressing GFP-PRMT1, Myc-RIPK1^{WT}, or Myc-RIPK1^{R658K}.

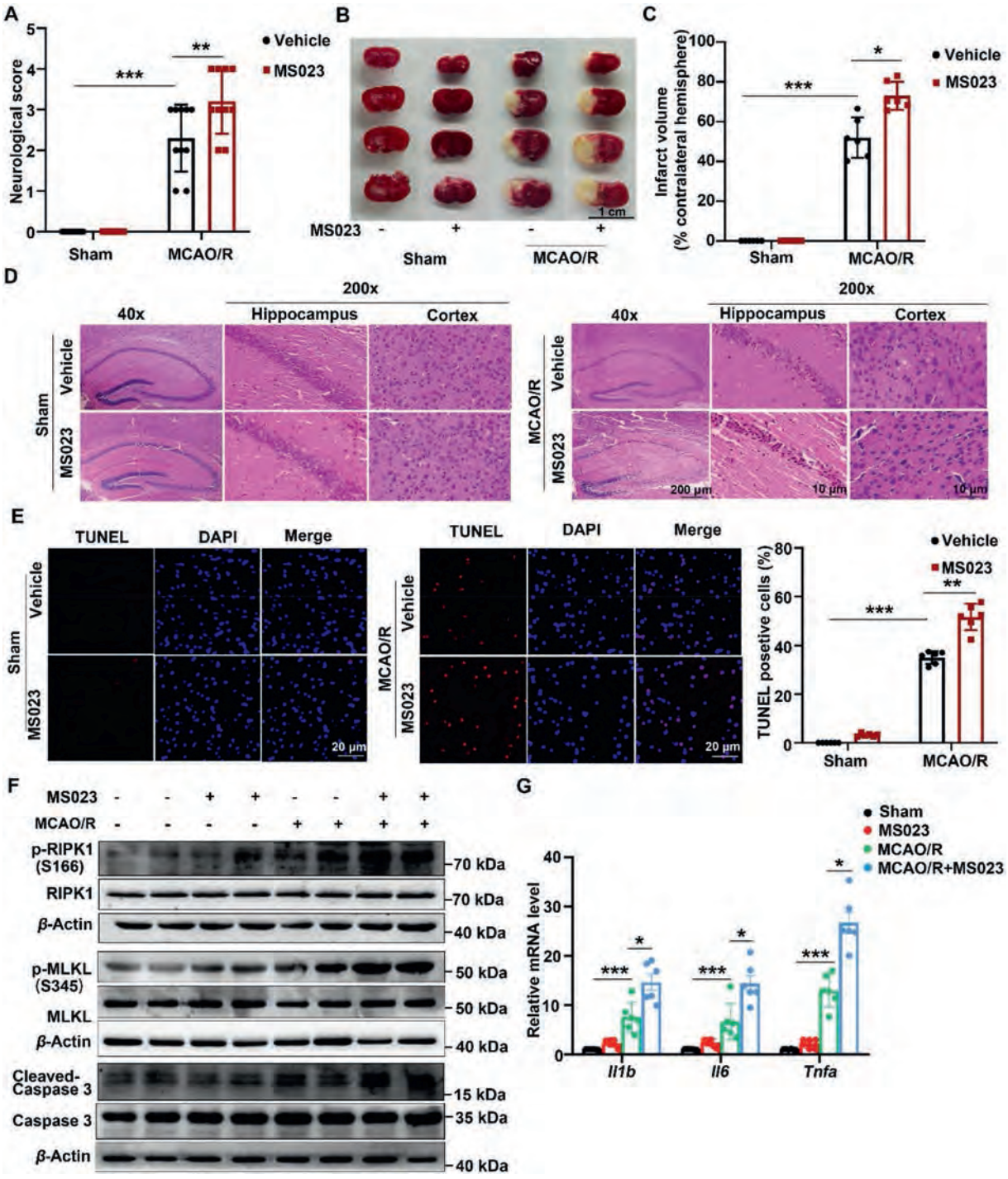

Figure 7 MS023 aggravated the cerebral I/R injury. Wild-type mice were subjected to MCAO for 2 h and reperfusion for 24 h. MS023 was intraventricularly administered to mice 30 min before MCAO. (A) Neurological deficit scores. $n = 10$ mice per group. (B) Representative photographs of coronal brain sections stained by TTC. Scale bar, 1 cm. (C) The infarct volume was expressed as the percentage of the contralateral hemispheric area. $n = 6$ mice per group. (D) Representative photomicrographs of H&E staining in the cortex and hippocampus. (E) Representative images and quantification of TUNEL staining in brain tissue. Scale bars, 20 μm. $n = 6$ mice per group. (F) Western blot analysis of p-RIPK1 (S166) and RIPK1, p-MLKL (S345) and MLKL, cleaved-caspase 3 and caspase 3 protein levels in I/R brain tissues. $n = 6$ mice per group. (G) The relative mRNA levels of *Il1b*, *Il6*, and *Tnfa* in brain tissues of mice subjected to ischemia−reperfusion injury. $n = 6$ mice per group. Results are shown as mean ± SD. Multiple comparisons were evaluated by two-way ANOVA followed by Tukey's test, $^{*}P < 0.05$, $^{**}P < 0.01$, $^{***}P < 0.001$ compared with indicated group.

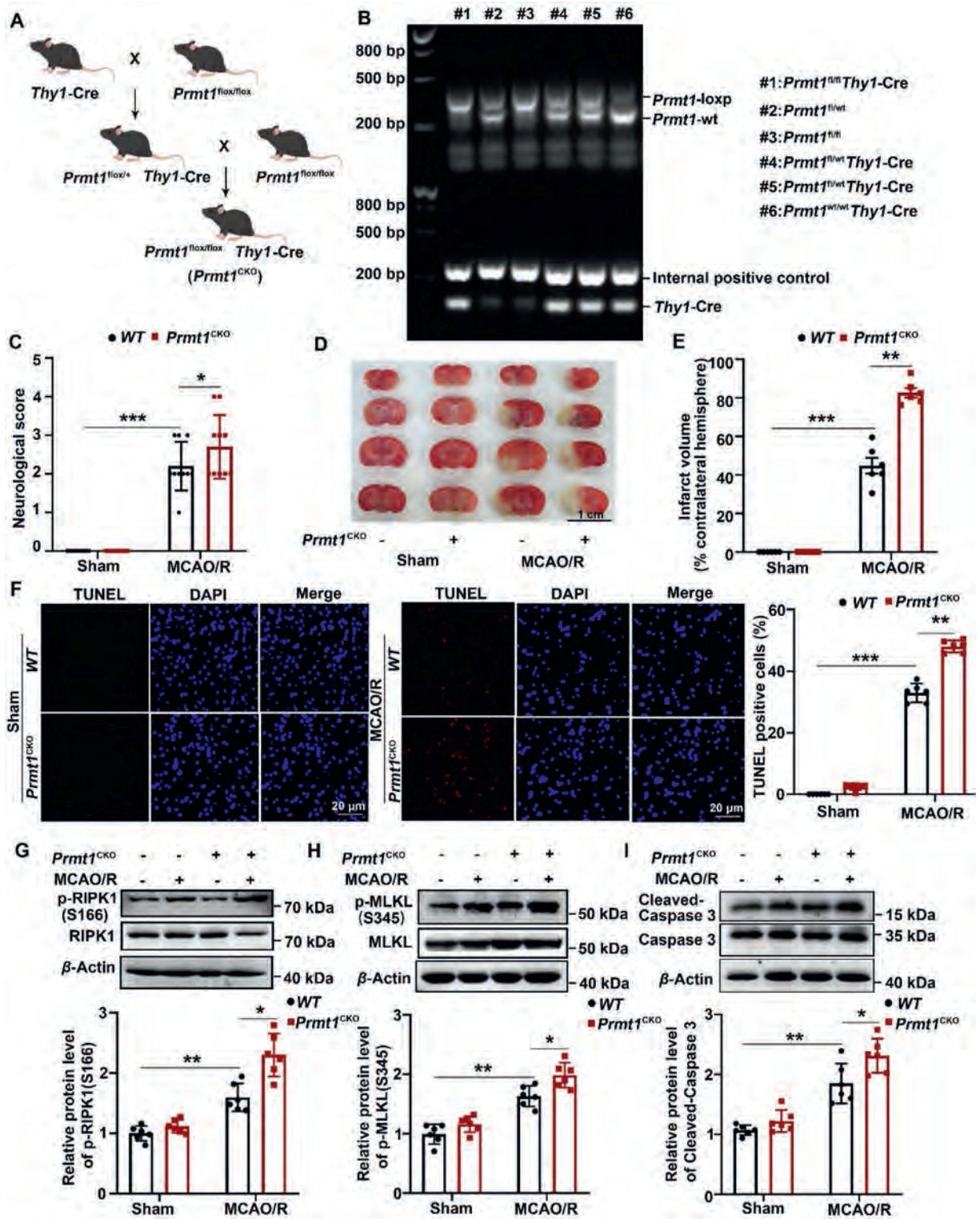

Figure 8 PRMT1 deficiency exacerbated the cerebral I/R injury. (A) *Prmt1*$^{flox/flox}$ mice were crossed with *Thy1*-Cre mice to generate *Prmt1*$^{flox/flox}$ *Thy1*-Cre mice. (B) Genotyping was confirmed by tail preparation and PCR at 3 weeks of age. (C) Neurological deficit scores. $n = 10$ mice per group. (D) Representative photographs of coronal brain sections stained by TTC. Scale bar, 1 cm. (E) The infarct volume was expressed as the percentage of the contralateral hemispheric area. $n = 6$ mice per group. (F) Representative images and quantification of TUNEL staining in brain tissue. Scale bars, 20 μm. $n = 6$ mice per group. (G−I) Western blot analysis of p-RIPK1 (S166) and RIPK1 (G), p-MLKL (S345) and MLKL (H), cleaved-caspase 3 and caspase 3 (I) protein levels in I/R brain tissues. $n = 6$ mice per group. Results are shown as mean ± SD. Multiple comparisons were evaluated by two-way ANOVA followed by Tukey's test, $^{*}P < 0.05$, $^{**}P < 0.01$, $^{***}P < 0.001$ compared with the indicated group.

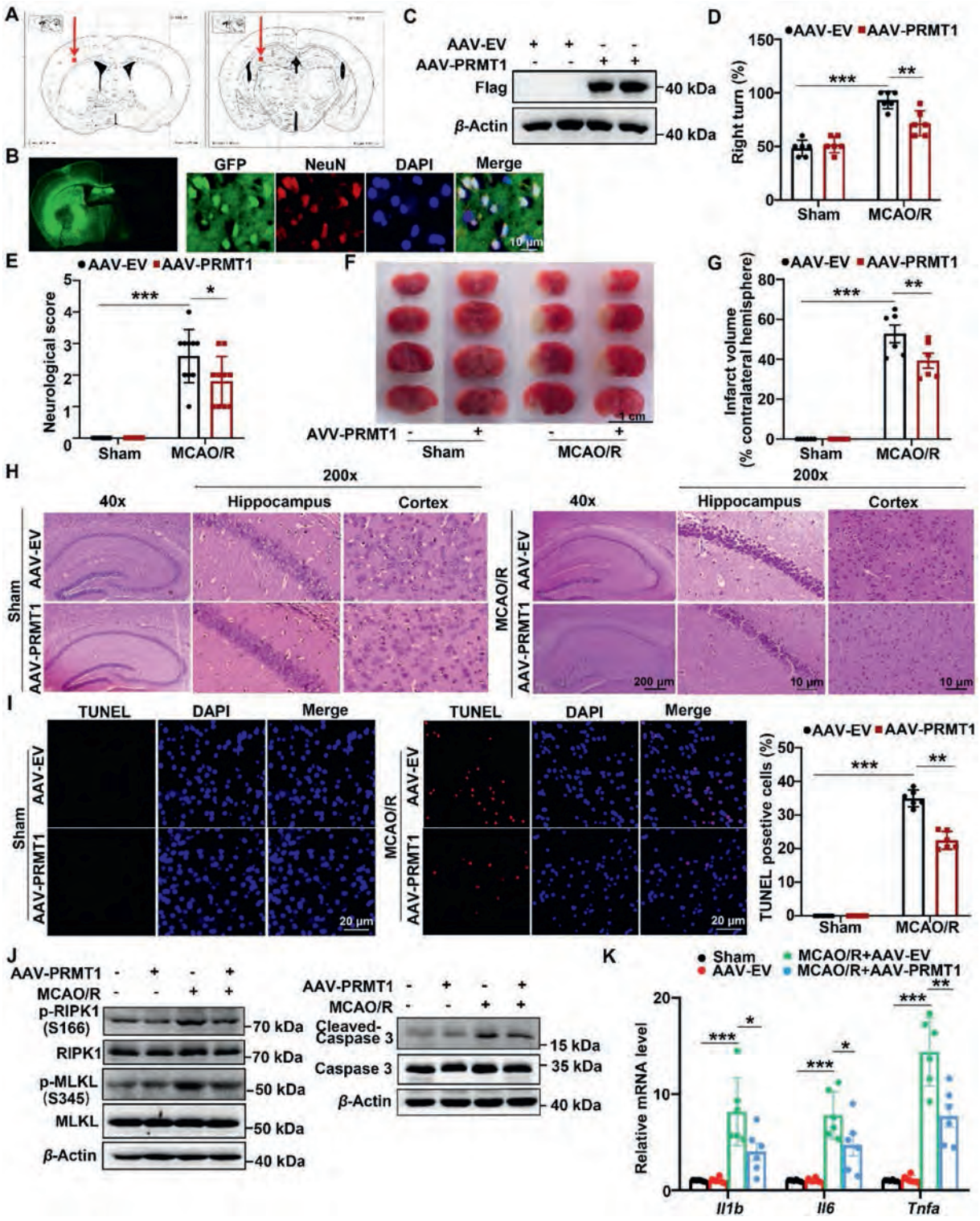

Figure 9 Overexpression of PRMT1 by AAV-PRMT1 injection ameliorated the cerebral I/R injury. Adeno-associated virus (AAV) containing PRMT1 (AAV-PRMT1) was injected into the left brain of WT mice for 3 weeks. Then the mice were subjected to MCAO for 2 h and reperfusion for 24 h. (A) The injection coordinates. The AAV-PRMT1 efficiently infected mouse brain (B) and the protein expression of PRMT1 (C) was elevated in the AAV-PRMT1-injected mice. (D) Corner test results of indicated mice subjected to MCAO/R or sham treatment in the left section of the brain. $n = 6$ mice per group. (E) Neurological deficit scores. $n = 10$ mice per group. (F) Representative photographs of coronal brain sections stained by TTC. Scale bars, 1 cm. (G) The infarct volume was expressed as the percentage of the contralateral hemispheric area. $n = 6$ mice per group. (H) Representative photomicrographs of H&E staining in the cortex and hippocampus. Scale bars, 20 μm. (I) Representative images and quantification of TUNEL assay in brain tissue. Scale bars, 20 μm. $n = 6$ mice per group. (J) Western blot analysis of p-RIPK1 (S166), RIPK1, p-MLKL (S345), MLKL, cleaved-caspase 3 and caspase 3 protein levels in I/R brain tissues. $n = 6$ mice per group. (K) The relative mRNA levels of *Il1b*, *Il6* and *Tnfa* in brain tissues of mice subjected to I/R injury. $n = 6$ mice per group. Results are shown as mean ± SD, multiple comparisons were evaluated by two-way ANOVA followed by Tukey's test, $^{*}P < 0.05$, $^{**}P < 0.01$, $^{***}P < 0.001$ compared with the indicated group.

whether PRMT1 is linked to the cerebral I/R injury is not clear. The present study showed that the total ADMA level and PRMT1 protein level were significantly decreased in the brain tissues subjected to MCAO/R, which was consistent with the results obtained in PC12 cells and cultured primary neurons. The details that the PRMT1 protein level was reduced after cerebral I/R injury were interesting and worth investigating. We found that PRMT1 mRNA levels barely changed in brain tissues of mice subjected to MCAO/R and it suggested the decrease of PRMT1 protein levels after cerebral I/R was not due to its transcriptional alteration. The ubiquitin-proteasome pathway is involved in the regulation of PRMT1 protein stability. The E3 ubiquitin ligases TRIM48, CHIP, E4B, and FBXO7 were all reported to polyubiquitinate PRMT1 and promote its degradation by the proteasome pathway[48-50]. Therefore, the downregulation of PRMT1 protein levels after cerebral I/R injury was possibly caused by its ubiquitin−proteasomal degradation. However, the specific E3 ligase mediated the degradation of PRMT1 in ischemic stroke needs further exploration. Notably, ADMA modification of RIPK1 was reduced in PC12 cells subjected to OGD/R. Moreover, p-RIPK1(S166), p-MLKL (S345), and cleaved-caspase 3 were upregulated at varying time points that are consistent with the previous report[9]. Based on the fact that PRMT1 mediated the ADMA modification of RIPK1 and inhibited its activation. Thus, we speculated that PRMT1 may be involved in cerebral I/R injury by regulating the kinase activity of RIPK1. Indeed, our results showed pharmacological inhibition of PRMT1 or PRMT1 deficiency notably facilitated the phosphorylation of RIPK1, accelerated the onset of apoptosis and necroptosis, and finally exacerbated the cerebral I/R injury. Inhibition of RIPK1 kinase activity by Nec-1 rescued the cell death induced by PRMT1 silence in OGD/R-treated PC12 cells. Hence, we demonstrated that PRMT1 was critical for both apoptosis and necroptosis by regulating the kinase activity of RIPK1 in cerebral I/R injury.

5. Conclusions

In this study, we identified PRMT1 as a regulator of RIPK1-dependent apoptosis and necroptosis after cerebral I/R injury. We provided evidence for the first time that PRMT1 directly targeted RIPK1 and mediated its ADMA modification, which inhibited the dimerization and phosphorylation of RIPK1, thus attenuating the RIPK1-dependent apoptosis and necroptosis. The cerebral I/R injury triggered the downregulation of PRMT1 which promoted the activation of RIPK1 and exacerbated the brain damage. Given the critical role of PRMT1 in cerebral I/R injury, PRMT1 would be an attractive therapeutic target for the treatment of stroke.

Acknowledgments

This work was supported by grants from the National Natural Science Foundation of China (Nos. 81971193 and 81873748) and Shandong Provincial Natural Science Foundation of China (ZR2023MH254 and ZR2022LZY025). We thank the Translational Medicine Core Facility of Shandong University for the consultation and instrument availability that supported this work.

Author contributions

Tengfei Liu: Writing − original draft, Validation, Methodology, Investigation. Gan Huang: Validation, Investigation. Xin Guo: Investigation, Writing − original draft. Qiuran Ji: Investigation, Methodology. Lu Yu: Investigation. Runzhe Zong: Investigation. Yiquan Li: Investigation. Xiaomeng Song: Software, Data curation. Qingyi Fu: Investigation. Qidi Xue: Investigation. Yi Zheng: Validation, Software, Methodology. Fanshuo Zeng: Validation, Methodology. Ru Sun: Validation, Methodology. Lin Chen: Visualization, Formal analysis, Data curation. Chengjiang Gao: Writing − review & editing, Supervision, Conceptualization. Huiqing Liu: Writing − review & editing, Supervision, Data curation, Conceptualization.

Conflicts of interest

The authors declare no competing interests.

Appendix A. Supporting information

Supporting information to this article can be found online at https://doi.org/10.1016/j.apsb.2025.06.005.

References

1. Iadecola C, Buckwalter MS, Anrather J. Immune responses to stroke: mechanisms, modulation, and therapeutic potential. *J Clin Investig* 2020;**130**:2777−88.
2. Iadecola C, Anrather J. Stroke research at a crossroad: asking the brain for directions. *Nat Neurosci* 2011;**14**:1363−8.
3. Gorelick PB. The global burden of stroke: persistent and disabling. *Lancet Neurol* 2019;**18**:417−8.
4. Tsivgoulis G, Saqqur M, Sharma VK, Brunser A, Eggers J, Mikulik R, et al. Timing of recanalization and functional recovery in acute ischemic stroke. *J Stroke* 2020;**22**:130−40.
5. Wang Q, Yang F, Duo K, Liu Y, Yu J, Wu Q, et al. The role of necroptosis in cerebral ischemic stroke. *Mol Neurobiol* 2024;**61**: 3882−98.
6. Degterev A, Huang Z, Boyce M, Li Y, Jagtap P, Mizushima N, et al. Chemical inhibitor of nonapoptotic cell death with therapeutic potential for ischemic brain injury. *Nat Chem Biol* 2005;**1**:112−9.
7. Ofengeim D, Yuan J. Regulation of RIP1 kinase signalling at the crossroads of inflammation and cell death. *Nat Rev Mol Cell Biol* 2013;**14**:727−36.
8. Yuan J, Amin P, Ofengeim D. Necroptosis and RIPK1-mediated neuroinflammation in CNS diseases. *Nat Rev Neurosci* 2019;**20**: 19−33.
9. Naito MG, Xu D, Amin P, Lee J, Wang H, Li W, et al. Sequential activation of necroptosis and apoptosis cooperates to mediate vascular and neural pathology in stroke. *Proc Natl Acad Sci U S A* 2020;**117**: 4959−70.
10. Deng XX, Li SS, Sun FY. Necrostatin-1 prevents necroptosis in brains after ischemic stroke *via* inhibition of RIPK1-mediated RIPK3/MLKL signaling. *Aging Dis* 2019;**10**:807−17.
11. Meng Y, Sandow JJ, Czabotar PE, Murphy JM. The regulation of necroptosis by post-translational modifications. *Cell Death Differ* 2021;**28**:861−83.
12. Laurien L, Nagata M, Schunke H, Delanghe T, Wiederstein JL, Kumari S, et al. Autophosphorylation at serine 166 regulates RIP kinase 1-mediated cell death and inflammation. *Nat Commun* 2020;**11**: 1747.
13. Tang Y, Tu H, Zhang J, Zhao X, Wang Y, Qin J, et al. K63-linked ubiquitination regulates RIPK1 kinase activity to prevent cell death during embryogenesis and inflammation. *Nat Commun* 2019;**10**: 4157.
14. Gerlach B, Cordier SM, Schmukle AC, Emmerich CH, Rieser E, Haas TL, et al. Linear ubiquitination prevents inflammation and regulates immune signalling. *Nature* 2011;**471**:591−6.

15. Wertz IE, O'Rourke KM, Zhou H, Eby M, Aravind L, Seshagiri S, et al. De-ubiquitination and ubiquitin ligase domains of A20 down-regulate NF-κB signalling. *Nature* 2004;**430**:694−9.
16. Draber P, Kupka S, Reichert M, Draberova H, Lafont E, de Miguel D, et al. LUBAC-recruited CYLD and A20 regulate gene activation and cell death by exerting opposing effects on linear ubiquitin in signaling complexes. *Cell Rep* 2015;**13**:2258−72.
17. Bedford MT, Clarke SG. Protein arginine methylation in mammals: who, what, and why. *Mol Cell* 2009;**33**:1−13.
18. Blanc RS, Richard S. Arginine methylation: the coming of age. *Mol Cell* 2017;**65**:8−24.
19. Yang Y, Hadjikyriacou A, Xia Z, Gayatri S, Kim D, Zurita-Lopez C, et al. PRMT9 is a type II methyltransferase that methylates the splicing factor SAP145. *Nat Commun* 2015;**6**:6428.
20. Nicholson TB, Chen T, Richard S. The physiological and pathophysiological role of PRMT1-mediated protein arginine methylation. *Pharmacol Res* 2009;**60**:466−74.
21. Hashimoto M, Murata K, Ishida J, Kanou A, Kasuya Y, Fukamizu A. Severe hypomyelination and developmental defects are caused in mice lacking protein arginine methyltransferase 1 (PRMT1) in the central nervous system. *J Biol Chem* 2016;**291**:2237−45.
22. Hashimoto M, Fukamizu A, Nakagawa T, Kizuka Y. Roles of protein arginine methyltransferase 1 (PRMT1) in brain development and disease. *Biochim Biophys Acta Gen Subj* 2021;**1865**:129776.
23. Amano G, Matsuzaki S, Mori Y, Miyoshi K, Han S, Shikada S, et al. SCYL1 arginine methylation by PRMT1 is essential for neurite outgrowth *via* Golgi morphogenesis. *Mol Biol Cell* 2020;**31**:1963−73.
24. Hofweber M, Hutten S, Bourgeois B, Spreitzer E, Niedner-Boblenz A, Schifferer M, et al. Phase separation of FUS is suppressed by its nuclear import receptor and arginine methylation. *Cell* 2018;**173**:706−19.
25. So HK, Kim H, Lee J, You CL, Yun CE, Jeong HJ, et al. *Protein arginine methyltransferase 1 ablation in motor neurons causes mitochondrial dysfunction leading to age-related motor neuron degeneration with muscle loss*, vol. 6. Research (Wash D C); 2023. p. 158.
26. Liu H, Wei X, Kong L, Liu X, Cheng L, Yan S, et al. NOD2 is involved in the inflammatory response after cerebral ischemia−reperfusion injury and triggers NADPH oxidase 2-derived reactive oxygen species. *Int J Biol Sci* 2015;**11**:525−35.
27. Zeng S, Zhao Z, Zheng S, Wu M, Song X, Li Y, et al. The E3 ubiquitin ligase TRIM31 is involved in cerebral ischemic injury by promoting degradation of TIGAR. *Redox Biol* 2021;**45**:102058.
28. Chen L, Kong L, Wei X, Wang Y, Wang B, Zhang X, et al. β-Arrestin 2 negatively regulates NOD2 signalling pathway through association with TRAF6 in microglia after cerebral ischaemia/reperfusion injury. *J Cell Mol Med* 2019;**23**:3325−35.
29. Modi J, Menzie-Suderam J, Xu H, Trujillo P, Medley K, Marshall ML, et al. Mode of action of granulocyte-colony stimulating factor (G-CSF) as a novel therapy for stroke in a mouse model. *J Biomed Sci* 2020;**27**:19.
30. Zhao Z, Song X, Wang Y, Yu L, Huang G, Li Y, et al. E3 ubiquitin ligase TRIM31 alleviates dopaminergic neurodegeneration by promoting proteasomal degradation of VDAC1 in Parkinson's disease model. *Cell Death Differ* 2024;**31**:1410−21.
31. Jin W, Zhao J, Yang E, Wang Y, Wang Q, Wu Y, et al. Neuronal STAT3/HIF-1α/PTRF axis-mediated bioenergetic disturbance exacerbates cerebral ischemia-reperfusion injury *via* PLA2G4A. *Theranostics* 2022;**12**:3196−216.
32. Yan Z, Wu H, Liu H, Zhao G, Zhang H, Zhuang W, et al. The protein arginine methyltransferase PRMT1 promotes TBK1 activation through asymmetric arginine methylation. *Cell Rep* 2021;**36**:109731.
33. Zheng S, Li Y, Song X, Wu M, Yu L, Huang G, et al. OTUD1 ameliorates cerebral ischemic injury through inhibiting inflammation by disrupting K63-linked deubiquitination of RIP2. *J Neuroinflammation* 2023;**20**:281.
34. Tang J, Frankel A, Cook RJ, Kim S, Paik WK, Williams KR, et al. PRMT1 is the predominant type I protein arginine methyltransferase in mammalian cells. *J Biol Chem* 2000;**275**:7723−30.
35. Eram MS, Shen Y, Szewczyk M, Wu H, Senisterra G, Li F, et al. A potent, selective, and cell-active inhibitor of human type I protein arginine methyltransferases. *ACS Chem Biol* 2016;**11**:772−81.
36. Wada K, Inoue K, Hagiwara M. Identification of methylated proteins by protein arginine *N*-methyltransferase 1, PRMT1, with a new expression cloning strategy. *Biochim Biophys Acta* 2002;**1591**:1−10.
37. Meng H, Liu Z, Li X, Wang H, Jin T, Wu G, et al. Death-domain dimerization-mediated activation of RIPK1 controls necroptosis and RIPK1-dependent apoptosis. *Proc Natl Acad Sci U S A* 2018;**115**:E2001−9.
38. Yin S, Liu L, Brobbey C, Palanisamy V, Ball LE, Olsen SK, et al. PRMT5-mediated arginine methylation activates AKT kinase to govern tumorigenesis. *Nat Commun* 2021;**12**:3444.
39. Mei X, Guo Y, Xie Z, Zhong Y, Wu X, Xu D, et al. RIPK1 regulates starvation resistance by modulating aspartate catabolism. *Nat Commun* 2021;**12**:6144.
40. Zhang T, Xu D, Liu J, Wang M, Duan LJ, Liu M, et al. Prolonged hypoxia alleviates prolyl hydroxylation-mediated suppression of RIPK1 to promote necroptosis and inflammation. *Nat Cell Biol* 2023;**25**:950−62.
41. Qin C, Yang S, Chu YH, Zhang H, Pang XW, Chen L, et al. Signaling pathways involved in ischemic stroke: molecular mechanisms and therapeutic interventions. *Signal Transduct Targeted Ther* 2022;**7**:215.
42. Tuo QZ, Zhang ST, Lei P. Mechanisms of neuronal cell death in ischemic stroke and their therapeutic implications. *Med Res Rev* 2022;**42**:259−305.
43. Dondelinger Y, Delanghe T, Priem D, Wynosky-Dolfi MA, Sorobetea D, Rojas-Rivera D, et al. Serine 25 phosphorylation inhibits RIPK1 kinase-dependent cell death in models of infection and inflammation. *Nat Commun* 2019;**10**:1729.
44. Jaco I, Annibaldi A, Lalaoui N, Wilson R, Tenev T, Laurien L, et al. MK2 phosphorylates RIPK1 to prevent TNF-induced cell death. *Mol Cell* 2017;**66**:698−710.
45. Geng J, Ito Y, Shi L, Amin P, Chu J, Ouchida AT, et al. Regulation of RIPK1 activation by TAK1-mediated phosphorylation dictates apoptosis and necroptosis. *Nat Commun* 2017;**8**:359.
46. Ganjam GK, Terpolilli NA, Diemert S, Eisenbach I, Hoffmann L, Reuther C, et al. Cylindromatosis mediates neuronal cell death *in vitro* and *in vivo*. *Cell Death Differ* 2018;**25**:1394−407.
47. Wang H, Meng H, Li X, Zhu K, Dong K, Mookhtiar AK, et al. PELI1 functions as a dual modulator of necroptosis and apoptosis by regulating ubiquitination of RIPK1 and mRNA levels of c-FLIP. *Proc Natl Acad Sci U S A* 2017;**114**:11944−9.
48. Hirata Y, Katagiri K, Nagaoka K, Morishita T, Kudoh Y, Hatta T, et al. TRIM48 promotes ASK1 activation and cell death through ubiquitination-dependent degradation of the ASK1-negative regulator PRMT1. *Cell Rep* 2017;**21**:2447−57.
49. Bhuripanyo K, Wang Y, Liu X, Zhou L, Liu R, Duong D, et al. Identifying the substrate proteins of U-box E3s E4B and CHIP by orthogonal ubiquitin transfer. *Sci Adv* 2018;**4**:e1701393.
50. Luo L, Wu X, Fan J, Dong L, Wang M, Zeng Y, et al. FBXO7 ubiquitinates PRMT1 to suppress serine synthesis and tumor growth in hepatocellular carcinoma. *Nat Commun* 2024;**15**:4790.